



Effect of reduction temperature of NiMoO_{3-x}/SAPO-11 on its catalytic activity in hydrodeoxygenation of methyl laurate



Ning Chen^a, Shaofeng Gong^b, Eika W. Qian^{a,*}

^a Graduate School of Bio-Applications and Systems Engineering, Tokyo University of Agriculture and Technology, Nakacho 2-24-16, Koganei, Tokyo 184-8588, Japan

^b Asia Petrochemical Supplies (Holdings), Tian He Bei Road 183, Tian He District, Guangzhou 510075, China

ARTICLE INFO

Article history:

Received 5 November 2014

Received in revised form 3 March 2015

Accepted 6 March 2015

Available online 10 March 2015

Keywords:

Hydrodeoxygenation

Isomerization

Methyl laurate

Nickel

Molybdenum oxides

Reduction temperature

ABSTRACT

To develop a non-sulfide and non-noble metal catalyst for the one step deoxygenation and isomerization of methyl laurate to hydrocarbons that are identical to diesel fuel, a SAPO-11 supported reduced nickel and molybdenum catalyst was prepared, and its performance was investigated after reduction pretreatment at various temperatures (400–550 °C). For comparison, sulfided NiMo/SAPO-11, reduced NiO/SAPO-11 and MoO₃/SAPO-11 were also studied. The reduction temperature exerted a significant influence on the deoxygenation activity, isomerization selectivity and deoxygenation pathway. The NiMo_{3-x}/SAPO-11 catalyst that was reduced at a lower temperature (400 °C) exhibited low deoxygenation activity but the highest isomerization selectivity. However, the activity subsequently increased over the catalyst reduced at 450 °C, and was higher than that of the sulfided catalyst. In addition, the isomerization selectivity decreased with increasing reduction temperature. The high activity and isomerization selectivity are ascribed to the increase in the density of surface species of Mo⁴⁺ and Mo⁵⁺, respectively. With regard to the deoxygenation pathway, the catalyst reduced at 400 °C exhibited a high decarbonylation selectivity that was similar to the nickel-catalyzed reaction. In contrast, the synergetic effect of the nickel metal and Mo⁴⁺ species can be responsible for the high selectivity toward hydrodeoxygenation over the catalyst reduced at higher temperatures (450–550 °C).

© 2015 Elsevier B.V. All rights reserved.

1. Introduction

Diesel range hydrocarbons produced from hydrotreating of triglycerides are considered to be one of the most promising energy carriers derived from vegetable oils [1,2]. Vegetable oils contain considerable amounts of oxygenates, such as triglycerides or free fatty acids. To convert these compounds into hydrocarbons identical to fossil-derived transportation fuels, the removal of oxygen atoms present in the vegetable oil is required. The commercial catalysts that applied in the hydrodeoxygenation of vegetable oil are commonly based on γ -Al₂O₃ supported molybdenum sulfide catalyst and promoted with lesser amounts of cobalt or nickel [3,4]. Because an external sulfur source should be used to maintain the active state of the sulfide catalyst [5], large amounts of sulfur species remain in the final products [6]. In fact, there are only trace amounts of sulfur (<10 ppm) in vegetable oils, and therefore, clean energy can easily be obtained without the hydrodesulfurization process compared to the energy derived from petroleum.

Based on this point of view, there is an apparent need to develop a non-sulfide catalyst for the hydrodeoxygenation of vegetable oils. The supported noble metal catalyst, such as Pd/SAPO-31 [7] or Pt/chloride Al₂O₃ [8], was utilized as a non-sulfide catalyst. Acid supports were employed to improve isomerization selectivity, and resulted in products with good cold flow properties [9]. However, the sintering of noble metals as well as their high cost become obstacles to their industrial utilize. In an effort to establish a more economical non-sulfide catalyst to upgrade vegetable oils, Lercher [10,11] and co-workers reported a new route for the conversion of microalgae oils into alkanes using ZrO₂-promoted Ni catalysts. Although these Ni-based catalysts have obvious advantages compared to previous catalysts, extremely high selectivity (>95%) toward decarboxylation/decarbonylation (DCO) was observed, resulting in a lower liquid yield than that over the sulfided catalyst. In addition, some gaseous products, i.e., CO and CO₂, were completely transformed to methane under the given reaction conditions due to the high methanation activity of the nickel phase, which increases the hydrogen consumption. Following work by the same group illustrated that selectivity toward the hydrodeoxygenation (HDO) pathway was achieved by changing the support to the acidic zeolite, i.e., HBEA and HZSM-5 [12,13]. Other

* Corresponding author. Tel.: +81 42 388 7410; fax: +81 42 388 7410.
E-mail address: whqian@cc.tuat.ac.jp (E.W. Qian).

groups demonstrated that the addition of P to the Ni catalyst [14,15] or the use of a bimetallic Mo–Ni catalyst [16] can also significantly promote the HDO pathway.

Recently, we designed a catalytic system with reduced Ni and MoO_{3-x} as the deoxygenation function combining with acid supports ($\text{SiO}_2\text{--Al}_2\text{O}_3$, SAPO-11 and AISBA-15) as the isomerization function to achieve a one-step process for the production of isomerized paraffins [13]. Higher isomerization and HDO selectivity were observed compared to those for the corresponding sulfided catalyst. However, a lower deoxygenation activity was observed, especially for the catalyst that used the SAPO-11 or AISBA-15 as a support, which have relatively high acidity. Perhaps the reduction difficulty depends on the interaction between the support and metal species, and higher acidity of support may result in an insufficient reduction. In addition, the deoxygenation mechanism and the reason for the low activity are not clear. Therefore, it is worthy from both the basic and applied point of view to obtain a more detailed understanding of the reactions involved in catalyst reduction.

In the present study, the hydrodeoxygenation of a model compound – methyl laurate (ML), was conducted using a fixed-bed continuous-flow reactor in the presence of NiMoO_{3-x} /SAPO-11 catalysts reduced at different temperatures. In addition, these catalysts were characterized using NO pulse chemisorption, transmission electron microscope (TEM), H_2 temperature-programmed reduction (H_2 -TPR), NH_3 temperature-programmed desorption (NH_3 -TPD) and X-ray photoelectron spectroscopy (XPS). The possible correlations among different valences of Mo species and the deoxygenation activity, the isomerization selectivity and the deoxygenation mechanism are discussed.

2. Experimental

2.1. Catalyst preparation

The nickel and molybdenum supported catalysts were prepared by a conventional incipient wetness impregnation method that was previously reported [14]. SAPO-11 zeolite with a one dimensional microporous structure ($6.5 \times 4.0 \text{ \AA}$) [15] has been considered to be the most promising support for isomerization of long chain paraffins due to its shape selectivity [16]. A SAPO-11 (Nikki-Universal Co., BET surface area: $175 \text{ m}^2/\text{g}$, $\text{Si}/\text{Al} = 0.1 \text{ mol/mol}$) sample was sieved to yield 425–850 μm particles, followed by drying at 120°C overnight. The SAPO-11 particles were then impregnated with the aqueous solution of $(\text{NH}_4)_6\text{Mo}_7\text{O}_{24} \cdot 4\text{H}_2\text{O}$ (Wako Pure Chem. Co., purity > 99.9%) and $\text{Ni}(\text{NO}_3)_2 \cdot 6\text{H}_2\text{O}$ (Wako Pure Chem. Co., purity > 99.9%) to achieve a loading amount of 20 wt% MoO_3 and 3.5 wt% NiO, in which Mo was introduced first. After each impregnation, the sample was dried at 120°C overnight and calcined at 450°C for 16 h in flowing air. Prior to analysis or reaction, the catalysts were activated by reduction with pure hydrogen (50 mL/min) at different temperatures ($400\text{--}550^\circ\text{C}$) for 3 h under near atmospheric pressure. For comparison, the prepared catalyst was activated by sulfidation with a mixture of 5 vol.% H_2S in H_2 (50 mL/min) at 100°C , 200°C and 300°C for 30 min and at 400°C for 3 h (referred as S–NiMo). In addition, $\text{NiO}/\text{SAPO-11}$ and $\text{MoO}_3/\text{SAPO-11}$ were also prepared. The reduced samples are denoted as xR–M, where x and M refer to the reduction temperature and metal, respectively.

2.2. Catalyst characterization

The textural properties of the support and catalysts were determined using the nitrogen adsorption–desorption isotherms at -196°C using a Belsorp-mini II automated sorption system. The specific surface area was calculated using the Brunauer–Emmett–Teller method [17] at a relative partial pressure of 0.05–0.3. The total pore volume and pore size distribution were

measured by a desorption curve using the Barre–Joyner–Halenda model [18] at a relative partial pressure of 0.95. Prior to the measurement, the samples were degassed under vacuum ($p < 10^{-2} \text{ kPa}$) at 400°C for 1 h.

The H_2 -TPR measurements were carried out using a ChemBET Pulsar TPR/TPD instrument (Quantachrome Instruments). The measured quantity of the calcined catalyst (ca. 100 mg) was loaded in a U shaped quartz tube. First, the sample was pretreated in a highly pure helium flow at 500°C for 3 h to remove any adsorbed impurities. Then, the sample was cooled to 30°C , followed by changing the gas to a 5 vol.% H_2 in argon gas mixture, which was introduced at a flow rate of 15 mL/min. H_2 -TPR was carried out by linearly increasing the temperature to 1000°C with a heating rate of $5^\circ\text{C}/\text{min}$. The water generated during the reduction was adsorbed on a column filled by soda lime. The hydrogen consumption was monitored using a thermal conductivity detector (TCD). A calibration curve for hydrogen was made for quantification. To obtain information regarding the reduction degree at different temperatures, an H_2 reduction experiment was performed under a constant temperature (at a heating rate of 20°C). The hydrogen consumption at a specific temperature was estimated by calculating the area of the reduction peak.

The acidity of the oxidized and reduced catalyst was measured by NH_3 -TPD using the same instrument as that used for H_2 -TPR [19]. Typically, a 200 mg sample was pre-reduced in situ in a hydrogen gas atmosphere (15 mL/min) for 3 h, followed by cooling to 30°C in a helium flow. The ammonia adsorption was conducted for 40 min under a 15 mL/min 10 vol.% NH_3 in helium gas mixture flow. The physically adsorbed ammonia was removed under helium flow at 100°C for 2 h, and the TPD was measured by linearly increasing the cell temperature from 100°C to 800°C at a heating rate of $10^\circ\text{C}/\text{min}$ under a 15 mL/min helium flow. Similarly, the amount of desorbed ammonia was monitored using a thermal conductivity detector (TCD) and quantified by pulse calibration.

The XPS spectra were acquired using an ESCA-3200 (Shimadzu) spectrometer with monochromatic Mg K α radiation (240 W, 8 kV, $E = 1253.6 \text{ eV}$). The spectrometer was interfaced to a SUN PC compatible for data collection. The CasaXPS software package (Casa Software Ltd., Teignmouth, UK) was used for subsequent data analysis. The binding energy (BE) values were referenced to the adventitious carbon (C 1s at 284.6 eV). A Shirley-type background was subtracted for Mo 3d envelopes, and the linear-type background was subtracted for Ni 2p envelopes. The recorded spectra were fitted using Gaussian–Lorentzian curves. The sample preparation was carried out in a dry box under an argon flow. A degassing pretreatment was carried out prior to analysis.

TEM was performed on a JEOL 2100 microscope (JEOL, Japan), working at 200 kV. Reduced sample was deposited on a carbon coated Cu grid.

NO pulse chemisorption was performed using the same instrument as that used for H_2 -TPR. 400 mg of the catalyst was used for each experiment. After reduction, the sample was further heated to 550°C under a helium flow to remove the hydrogen adsorbed on the surface, followed by cooling to 40°C for pulse adsorption. Helium was used as the carrier gas, and successive doses of 10% NO/He gas were subsequently introduced using a calibrated injection valve ($25 \mu\text{L NO pulse}^{-1}$).

2.3. Catalytic testing

The hydrodeoxygenation of methyl laurate (Tokyo Chem. Ind., purity > 98%) was chosen as a model reaction to evaluate the deoxygenation and isomerization activity of the catalysts. These reactions were performed in a high-pressure fixed-bed continuous-flow stainless steel reactor (8 mm in diameter and 40 mm in length), operated in the down-flow mode [20]. For the activity test, 1.5 g

Table 1

Textural and structural characteristics of the support and catalysts.

Sample	NiO ^a (wt.%)	MoO ₃ ^a (wt.%)	S _{BET} ^b (m ² /g)	d _p ^c (nm)	V _p ^d (cm ³ /g)
SAPO-11	–	–	167	5.8	0.24
NiO/SAPO-11	3.5	–	126	7.0	0.22
MoO ₃ /SAPO-11	–	19.5	94	7.9	0.19
NiMo/SAPO-11	3.3	18.3	52	9.6	0.12
400R–NiMo	–	–	75	6.3	0.12
450R–NiMo	–	–	74	6.3	0.12
500R–NiMo	–	–	76	6.5	0.13
550R–NiMo	–	–	79	6.6	0.13

^a Chemical composition determined by XRF.^b Specific surface area.^c Average pore diameter.^d Pore volume.

of the calcined catalyst was diluted with quartz and charged into the reactor. To investigate the effect of reduction temperature, the catalysts were reduced in situ at the individual desired temperature for 3 h under a 50 mL/min H₂ flow. The reactions were conducted at different temperatures (275–375 °C), under 3 MPa of hydrogen pressure, with a weight hourly space velocity (WHSV) of 5 h^{−1} and a H₂/feed ratio of 800 (v/v). The catalytic activity was measured after the catalyst stabilized (from TOS = 5 h). No significant deactivation of the catalyst was observed during any of the experiments. After the reaction, the liquid products were diluted with carbon tetrachloride and analyzed using a gas chromatograph (GC-2025, Shimadzu Corp.) equipped with a flame ionization detector (FID) and a DB-5HT column (Agilent, 30 m × 0.25 mm i.d., 0.25 μm). The product identification was performed using a gas chromatograph–mass spectrometer (GC–MS–QP5050A, Shimadzu Corp.) equipped with the same capillary column. Another gas chromatograph with a thermal conductivity detector (TCD) and a Unibeads C column (GL Sciences Inc., 3 m × 3 mm i.d.) was used to measure other components, such as CO and CO₂, in the gaseous products.

The amount of products was quantified using GC standards. The conversion of methyl laurate, deoxygenation degree and selectivity were calculated as follows:

$$\text{Conversion (\%)} = \left(1 - \frac{n_{\text{ML}}}{n_{\text{MLO}}}\right) \times 100$$

$$\text{HDO (\%)} = \left(1 - \frac{\sum \text{Product}}{\sum \text{Feedstock}}\right) \times 100$$

$$\text{Selectivity (\%)} = \frac{n_i \times a_i}{\sum n_i \times a_i} \times 100$$

where n_{MLO} is the number of molecules of ML in the feedstock, n_{ML} is the number of molecules of ML in the product, $\sum \text{Feedstock}$ is the molar amount of total oxygen in the feedstock, $\sum \text{Product}$ is the molar amount of total oxygen in the products, n_i is the mole number of product i , and a_i is the carbon atom number of product i . The turnover frequency was determined using the following equation:

$$\text{TOF} = -\frac{F/W}{M} \times \ln(1 - X)$$

where X is the conversion (%), F is the reactant molar flow (mol/s), W is the catalyst weight (g) and M is number of the active sites measured by NO pulse chemisorption.

3. Results

3.1. Catalyst characterization

3.1.1. Textural properties

The textural properties of the support and catalyst are listed in Table 1. After metal incorporation, both the surface area and pore volume decreased due to the location of the active phase. After reduction, there is a little increase in the BET surface area, but no considerable variation was observed among the catalysts reduced at different temperatures. Chemical composition results obtained by X-ray fluorescence analysis indicate that the active metal was successfully loaded for each sample.

3.1.2. H₂-TPR

H₂-TPR patterns for the NiO/SAPO-11, MoO₃/SAPO-11 and NiMo/SAPO-11 catalysts are compared in Fig. 1. The reduction peaks appeared in two regions; one started at 400 °C and ended at 720 °C, and the other one was observed at a higher temperature. For NiO/SAPO-11, the lower temperature reduction peak was due to the reduction of bulk nickel oxide species with less interaction with SAPO-11, and the higher one was attributed to the dispersed nickel. In addition, the reduction peak at temperatures higher than 900 °C may correspond to the reduction of nickel aluminate (NiAl₂O₄) [21,22]. For MoO₃/SAPO-11, the maximum hydrogen consumption was observed at 652 °C, which was assigned to the reduction of Mo⁶⁺ in octahedral coordination to Mo⁵⁺ and Mo⁴⁺. Another reduction peak at temperatures higher than 900 °C corresponded to the further reduction of Mo⁴⁺, to form lower molybdenum oxidation state, such as Mo²⁺ or zerovalent molybdenum species. For NiMo/SAPO-11, the TPR profile exhibited two reduction peaks in region I, i.e., one at 612 °C and another shoulder peak at 551 °C.

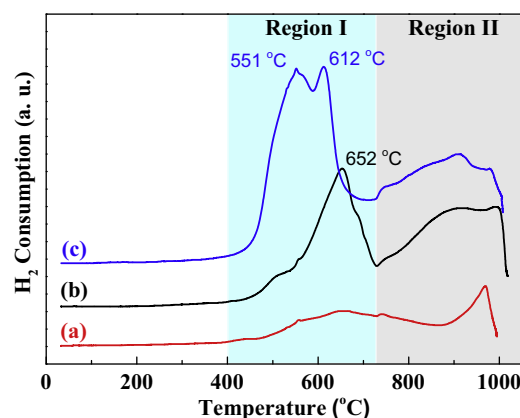


Fig. 1. H₂-TPR profiles of (a) NiO/SAPO-11, (b) MoO₃/SAPO-11 and (c) NiMo/SAPO-11.

Table 2
Hydrogen consumption of the catalysts during H₂-TPR.

Reduction temperature (°C)	H ₂ consumption (mmol/g)		
	NiMo/SAPO-11	MoO ₃ /SAPO-11	NiO/SAPO-11
Hydrogen consumption calculated from H ₂ -TPR			
Region I	0.15	0.10	0.05
Region II	0.11	0.09	0.03
Region I + II	0.26	0.19	0.08
Hydrogen consumption estimated at different reduction temperatures			
400 °C	0.05	0.02	0.01
450 °C	0.15	0.03	0.02
500 °C	0.17	0.06	0.03
550 °C	0.18	0.10	0.04
600 °C	0.18	0.10	0.04

The latter peak was attributed to the reduction of MoO₃, and the former peak was due to the reduction of nickel oxide and a portion of the molybdenum oxide. Interestingly, the reduction peak of NiMo/SAPO-11 in region I shifted to a lower temperature side compared to that of Mo/SAPO-11. This result can be explained by the hydrogen spillover from nickel to molybdenum [23], which promoted the reduction rate of molybdenum oxide.

The hydrogen consumption results estimated from the calibration curve are listed in Table 2. For region I, the aggregate hydrogen consumption of NiO/SAPO-11 and MoO₃/SAPO-11 was consistent with that of NiMo/SAPO-11, indicating that nearly all of the NiO species in NiMo/SAPO-11 were reduced to nickel metal in this region. For region II, the hydrogen consumption of MoO₃/SAPO-11 was similar to that of NiMo/SAPO-11, suggesting that the reduction degree was not improved by nickel addition.

To further investigate the reduction degree of the catalyst, hydrogen reduction profiles were recorded at a constant temperature (Fig. S2). It should be noted that in every case the final temperature had been reached prior to the appearance of the hydrogen consumption peak due to the high heating rate (20 °C/min). The reduction degree derived from different temperatures is listed in Table 2. For NiMo/SAPO-11, a nearly threefold increase was observed when the reduction temperature increased from 400 to 450 °C. However, only a slight increase was observed above 450 °C. In contrast, the reduction degree of NiO/SAPO-11 and MoO₃/SAPO-11 exhibited tendency to continuous increase with an increasing reduction temperature.

3.1.3. NH₃-TPD

The acidity of the support, oxidic and reduced catalysts was determined by NH₃-TPD, and the desorption profiles are shown in Fig. 2. All of the studied samples exhibited similar TPD profiles with two distinct desorption peaks centered at approximately 260 °C and 350 °C, which respectively correspond to weak and medium acid sites primarily originate from SAPO-11. In addition, another peak emerged at ca. 550 °C was observed for the catalyst reduced at 400, 450 or 500 °C. However, this peak was not observed for the support, oxidized catalyst or catalyst reduced at 550 °C. This result indicates that new acid sites were generated after reduction at 400–500 °C. To compare the number of acid sites, the NH₃ desorption peak was divided into two or three regions, and the acidity of each individual region is listed in Table 3. The number of total acid sites substantially increased after impregnating the NiMo metals. However, it decreased gradually as the reduction temperature increased. The number of new acid sites observed at the desorption temperatures higher than 400 °C also decreased as the reduction temperature increased. Suarez et al. [24] studied the acidic properties of Mo/Al₂O₃ reduced to different extents by infrared spectroscopy of adsorbed pyridine. Two interesting conclusions provide evidence to explain the variation in our NH₃-TPD

results. First, the IR spectroscopy showed the presence of Brønsted acid sites on the oxidized catalyst but not on the alumina. Second, the Brønsted acid sites increased at low extents of reduction and decreased to zero with further reduction. However, the Lewis acidity passed through a maximum as a function of the reduction degree but was not eliminated with reduction. In this study, the increase in the number of acid sites after impregnation may be related to both of the Brønsted and Lewis acid sites that were generated by molybdenum oxide. However, the decrease in these sites was due to the gradual elimination of Brønsted acid sites. The new acid sites generated after reduction may correspond to hydroxide groups bond to Mo⁵⁺ species.

3.1.4. XPS

XPS study was conducted to determine the oxidation states of the metal after different reduction processes. Fig. 3 shows the Mo 3d curve-fitted spectra for the reduced NiMo/SAPO-11 catalysts. Three sets of Mo 3d doublets were observed: Mo⁶⁺, Mo⁵⁺ and Mo⁴⁺. Yamada et al. [25] studied the distribution of molybdenum oxidation states in reduced Mo/γ-Al₂O₃ and found that Mo³⁺ was obtained after 500 °C reduction. However, other results [26,27] indicate that no valence lower than +4 was obtained at the same reduction temperature. Based on these results, the reduction degree of molybdenum is strongly dependent on the preparation method and acidity of the support. Therefore, the interaction between the metal and support would change the reduction difficulty. In this sense, the Brønsted acid sites in SAPO-11 caused more difficulties for the reduction of supported molybdenum oxide. The binding energies (BE) and relative abundance of each Mo oxidation state are listed in Table 4. The BE value for the Mo⁶⁺ was obtained from the XPS spectra of oxidic catalyst (Mo 3d_{5/2}, 232.9 eV; Mo 3d_{3/2}, 236.0 eV). A good agreement with the BE values is observed in other literatures [25–29]. The XPS parameters for Mo⁵⁺ and Mo⁴⁺ were a result of the curve fitting procedure. For the 500R–NiMo and 550R–NiMo catalysts, the BE of Mo⁵⁺ and Mo⁴⁺ shifted to lower values compared to 400R–NiMo and 450R–NiMo, suggesting that a higher reduction degree was obtained and more coordinately unsaturated sites (CUS) were generated. The relative concentration of each Mo oxidation state was calculated by dividing the Mo 3d area for a given oxidation state by the total area of the Mo 3d envelope. The concentration of Mo⁵⁺ or Mo⁴⁺ species exhibited a significant change in the different catalysts. The percentage of Mo⁴⁺ exhibited a steady increase from 29.2% to 51.4% with increasing reduction temperature, whereas that of Mo⁵⁺ dropped from an initial high value of 43.5% to 20.0%. These result indicates that a higher temperature favors the formation of a lower valence of Mo⁴⁺

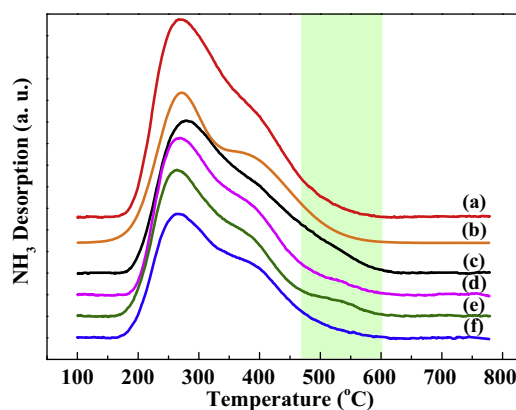
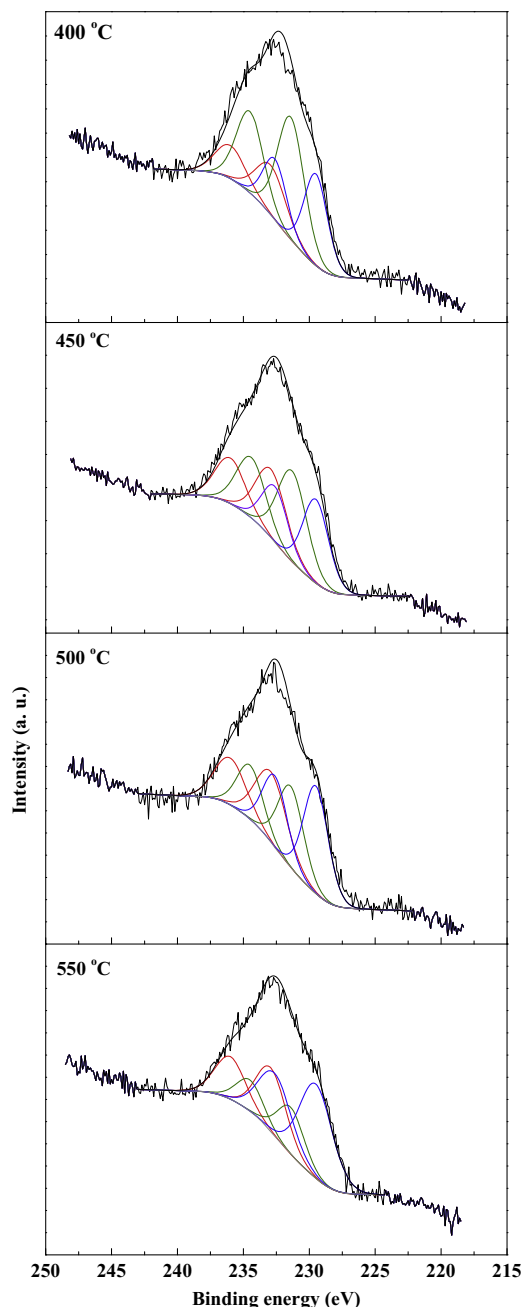


Fig. 2. NH₃-TPD profiles of (a) oxidic NiMo/SAPO-11, (b) SAPO-11 and NiMo/SAPO-11 reduced at (c) 400 °C, (d) 450 °C, (e) 500 °C and (f) 550 °C. The colored area shows the third ammonia desorption peak corresponding to the new acid sites.

Table 3
Acidity of the support and catalysts determined by NH_3 -TPD.

Sample	Weak		Medium		Strong		Total acidity ($\mu\text{mol/g}$)
	T/ $^\circ\text{C}$	Acidity ($\mu\text{mol/g}$)	T/ $^\circ\text{C}$	Acidity ($\mu\text{mol/g}$)	T/ $^\circ\text{C}$	Acidity ($\mu\text{mol/g}$)	
SAPO-11	265	160.0	370	265.8	–	–	425.8
Oxidized	266	206.9	361	324.0	–	–	530.9
400R–NiMo	261	122.5	322	151.3	416	193.7	467.5
450R–NiMo	262	144.4	341	194.2	436	101.4	440.0
500R–NiMo	258	147.5	345	204.4	472	47.1	399.0
550R–NiMo	262	121.0	361	232.2	–	–	353.2

**Fig. 3.** XPS spectra of the Mo 3d region for NiMo/SAPO-11 reduced at different temperatures.

rather than Mo^{5+} . Many studies investigated the reduction kinetics of supported MoO_3 [30,31], and the results indicated that different valences of molybdenum oxides showed quite different distributions in the initial state of reduction, but they could remain the same

after a certain time period (approximately 3–5 h). In this study, a sufficient time of 3 h was maintained for each reduction process. Therefore, the final oxidation state was reached in each case, and the reduction degree only depends on the reduction temperature. On the other hand, the Mo^{6+} showed a constant concentration in the different catalysts. These Mo^{6+} species strongly interacted with the support and required a higher energy for reduction.

The XPS spectra for Ni 2p are shown in Fig. 4. For oxidized NiMo/SAPO-11, the peak at 858.3 eV was due to NiO. After reduction, the value of the binding energy shifted to lower side (854.8 eV), and only zerovalent nickel was observed in each case, indicating that the nickel oxide on the surface of NiMo/SAPO-11 was completely reduced even when the temperature was relatively low (400 $^\circ\text{C}$), which correlates well with the H_2 -TPR results.

3.1.5. TEM

TEM images of the reduced NiMo/SAPO-11 catalysts are displayed in Fig. 5. The average size of 400R–NiMo was ca. 9.1 nm. The increase in the reduction temperature only resulted in a slight migration of the metal particles, and the average particle size of the 550R–NiMo was estimated to be 10.2 nm. Based on these results, it can be concluded that the reduction temperature cannot significantly influence the particle size of metal.

3.1.6. NO pulse chemisorption

NO is frequently used for quantifying the active sites in hydrotreating catalysts. It is widely accepted that NO can be used to probe the anion vacancies, i.e., the CUS sites, on (Ni/Co)MoS [32,33] or reduced NiMo [34] system. In general, NO is considered to be adsorbed as dinitrosyl species on Mo^{4+} and Ni species [35]. The NO uptake for the reduced catalysts is listed in Table 5. The adsorption amount of NO for the reduced NiMo/SAPO-11 catalyst gradually increased with the increasing reduction temperature. Based on the TEM result, the average particle size for these catalysts was similar, indicating that the metal dispersion cannot be changed considerably by the reduction at different temperatures. Therefore, the reason for the variation in NO adsorption amount may be due to an increase in the CUS sites. In addition, the monometallic Mo/SAPO-11 catalyst possessed lower NO adsorption capacity,

Table 4
Binding energy and distribution of molybdenum species on the reduced catalysts.

Sample	Binding energy ^a (eV)			Concentration ^b (%)		
	Mo^{6+}	Mo^{5+}	Mo^{4+}	Mo^{6+}	Mo^{5+}	Mo^{4+}
400R–NiMo	232.9	231.4	229.5	28.9	43.5	27.6
450R–NiMo	232.9	231.3	229.5	28.1	34.4	37.5
500R–NiMo	232.9	231.1	229.1	28.6	30.1	41.3
550R–NiMo	232.9	231.1	229.1	28.6	20.0	51.4

^a The value of binding energy referred to Mo $3d_{5/2}$. The difference between the binding energy value of $3d_{5/2}$ and $3d_{3/2}$ was kept constant (3.1 eV) for all oxidation states.

^b Concentration of different valences of molybdenum species was obtained from the areal percentage.

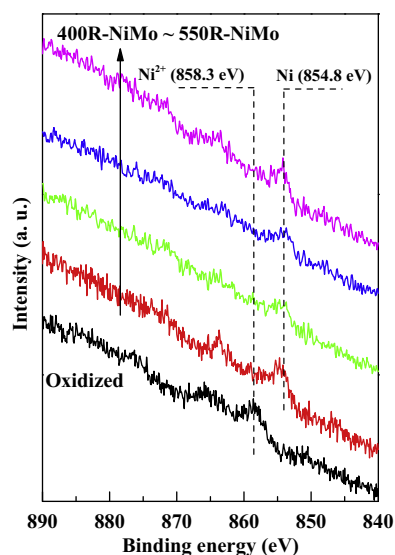


Fig. 4. Ni 2p envelopes for the oxidized and reduced NiMo/SAPO-11 catalyst.

while the Ni/SAPO-11 catalyst exhibited much higher NO adsorption amount than the other catalysts.

3.2. Hydrodeoxygenation of methyl laurate

A typical chromatogram of the liquid products (diluted with carbon tetrachloride) displaying peaks of solvent, unreacted reactant and products of HDO of ML is shown in Fig. S1. The HDO of ML resulted in the formation of two types of liquid products, i.e., oxygenates and hydrocarbons. The main hydrocarbons were dodecane

and undecane. In addition, hydrocarbons with a carbon number less than 10 were observed at a higher temperature (375 °C), and are considered to be the cracking products. For the oxygenate, dodecanol, dodecanal, laurate acid and lauryl laurate were observed as intermediate products at low temperatures, and these compounds were further transformed into hydrocarbons with the increasing reaction temperature. Moreover, a small amount of methanol was also detected, and the amount of methanol decreased as the reaction temperature increased. In each case, water formation was observed in addition to the other liquid organic products. These results were consistent with other literatures that used triglyceride [36], fatty acid [10] or fatty acid methyl ester [37,38] as the feedstock. With regard to the gaseous products, CH₄ and CO were observed as the main products. In addition, a small amount of CO₂ was observed at the reaction temperature higher than 325 °C. Interestingly, a small amount of dimethyl ether was detected and the amount was decreased as the temperature increased, indicating that dimethyl ether was formed by the reaction of the intermolecular dehydration of methanols, which was favored at lower temperatures.

3.3. HDO of methyl laurate over different reduced catalysts

The HDO reactions of ML over the NiMo/SAPO-11 catalyst reduced at different temperatures were conducted under the following reaction conditions: $T=275$ to 375 °C, WHSV = 5 h^{-1} , $P=3$ MPa, and $\text{H}_2/\text{Feed}=800\text{ ml/ml}$ to investigate the effects of reduction temperature. Fig. 6 shows the effect of the reduction temperature on the catalyst activity. The catalyst reduced at 400 °C exhibited the lowest activity, and the ML conversion over this catalyst was much lower than that over the sulfided catalyst (see in Table S1) at reaction temperatures of 275–350 °C. When the

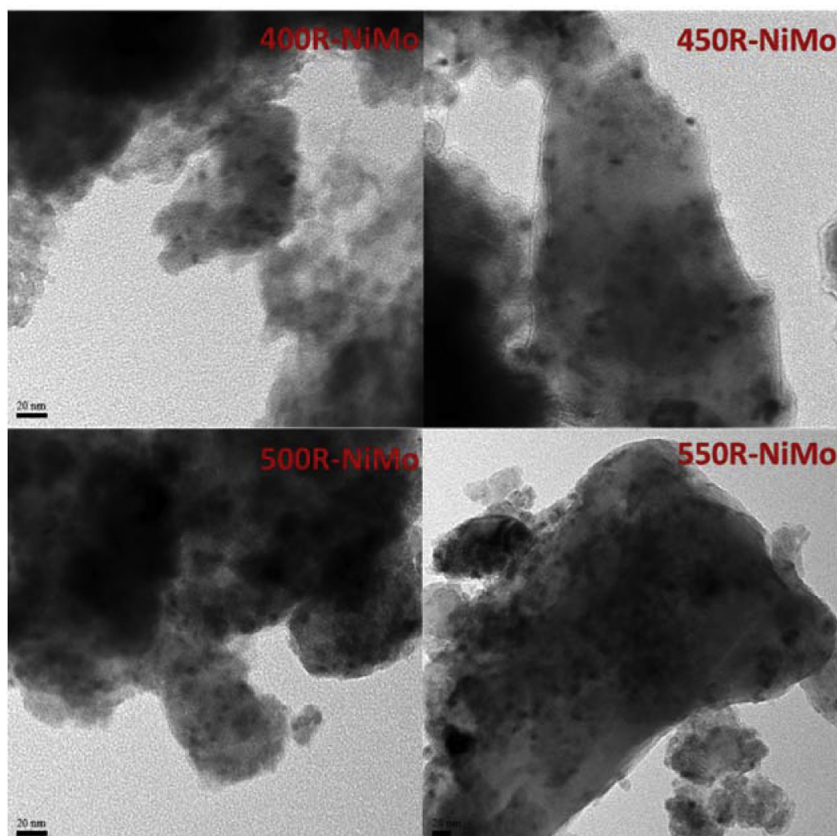


Fig. 5. TEM micrographs of the NiMo/SAPO-11 catalyst reduced at different temperatures.

Table 5

Transformation of methyl laurate over various catalysts at 275 and 300 °C.

	500R–Ni		550R–Mo		400R–NiMo		450R–NiMo		500R–NiMo		550R–NiMo	
	275 ^f	300 ^f	275 ^f	300 ^f	275 ^f	300 ^f	275 ^f	300 ^f	275 ^f	300 ^f	275 ^f	300 ^f
Conv. ^a (%)	19.2	74.1	30.8	49.5	15.0	27.3	46.8	69.9	46.2	68.4	50.78	75.72
NO ad. ^b (μmol/g)	462		197		171		225		230		275	
TOF ^c (10 ^{−3} /g)	0.64	4.06	2.59	4.81	1.32	2.59	3.89	7.42	3.74	6.96	3.58	7.15
DCO ^d (mol %)	19.9	24.1	0.5	0.9	3.0	5.6	2.4	4.7	2.3	5.0	2.6	6.4
HDO ^d (mol %)	6.4	68.1	17.6	41.3	5.1	10.4	13.1	36.2	13.6	44.0	18.1	65.1
DCO/HDO ^e	3.11	0.35	0.03	0.02	0.59	0.54	0.18	0.13	0.17	0.11	0.14	0.10

^a Conversion of methyl laurate.^b NO adsorption was measured by NO pulse chemisorption at 40 °C.^c Turnover frequency, defined as reacted methyl laurate molecules per active site per second.^d DCO and HDO represented the selectivity to C₁₁ and C₁₂ hydrocarbons, respectively.^e Molar ratio between DCO and HDO.^f Reaction temperature (°C).

reduction temperature increased to 450 °C, the activity increased dramatically and was higher than that of the sulfided one. However, above 450 °C, only a slight increase in the conversion was observed. In addition, the conversion was close to 100% at a higher reaction temperature (375 °C).

In Fig. 7, the liquid product distribution and isomerization selectivity over different reduced catalysts are compared. At a lower reaction temperature (275 °C), the main products over the four catalysts were oxygenates, especially lauryl laurate. Other oxygenates such as dodecanol, dodecanal and laurate acid were observed in trace amounts. At 325 °C, C₁₁ and C₁₂ hydrocarbons were observed as the main products over the catalyst reduced at higher temperatures (450–550 °C). However, oxygenates were also observed in large quantities over the catalysts reduced at 400 °C. This result is consistent with the ML conversion, in which catalyst reduced at 400 °C showed the lowest activity. At a higher reaction temperature (375 °C), oxygenates were barely observed in each case. For the C₁₁ and C₁₂ hydrocarbons, the formation of C₁₁ was favored at a higher reaction temperature. On the other hand, the isomers selectivity (*iso*-C₁₁ and *iso*-C₁₂) increased with increasing reaction temperature. Interestingly, the isomers selectivity remained constant among the different catalysts at a reaction temperature of 325 °C, but this selectivity was altered at 375 °C. It is important to note that in the HDO of ML, deoxygenation and isomerization were consecutive reactions because no isomerized oxygenates were observed in the products [19,20]. Therefore, the deoxygenation degree has a large influence on the isomerization, that is, the deoxygenation is a prerequisite for subsequent isomerization. In this sense, isomerization was substantially inhibited by the low hydrocarbons formation over the 400R–NiMo at 325 °C. In addition, the formation of the C₅–C₁₀ hydrocarbons as well as the gaseous

cracking products (C₂–C₄, not shown) was lower than 5% in every case even though the reaction temperature was increased to 375 °C. To investigate the effect of the reduction temperature on the isomerization selectivity, the ratio of isomerized to normal paraffins is shown in Fig. 8. The isomerization selectivity increased with increasing reaction temperature, but it decreased with increasing reduction temperature. At lower reaction temperatures, i.e., 275 and 300 °C, only trace amounts of the isomers (<2%) were generated, resulting in a ratio close to zero. When the reaction temperature was higher than 325 °C, 400R–NiMo exhibited a much

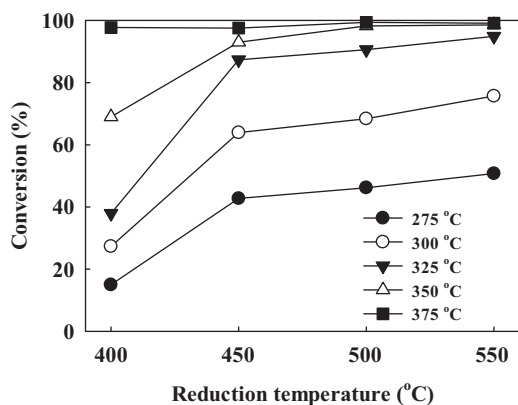


Fig. 6. Effect of the reduction temperature on the conversion over the NiMo/SAPO-11 catalyst at a reaction temperature of 275–375 °C.

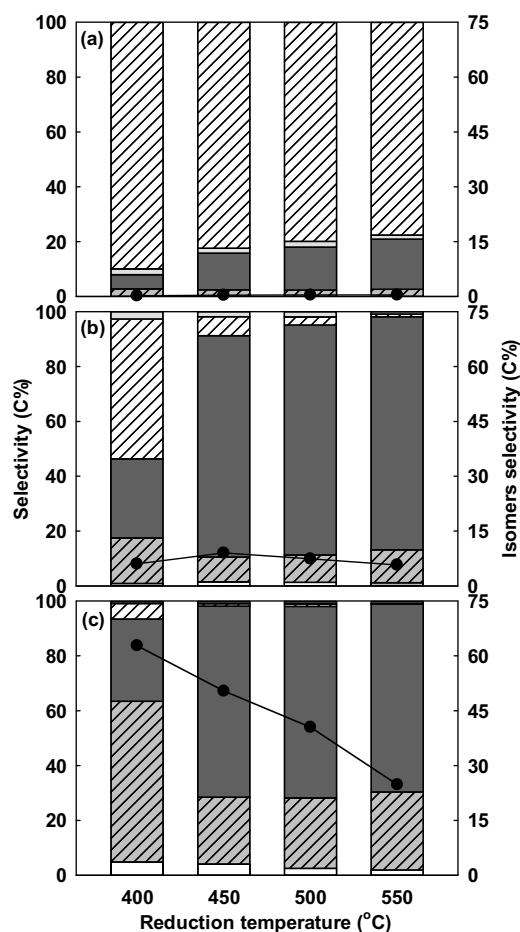


Fig. 7. Effect of the reduction temperature on the liquid product distribution (□ C₅–10 hydrocarbons, ▨ C₁₁ hydrocarbons, ■ C₁₂ hydrocarbons, ▤ Oxygenates, ▩ C₁₂+) and isomer selectivity at (a) 275 °C, (b) 325 °C, (c) 375 °C. The black circle represents the isomer selectivity and can be read on the right axis.

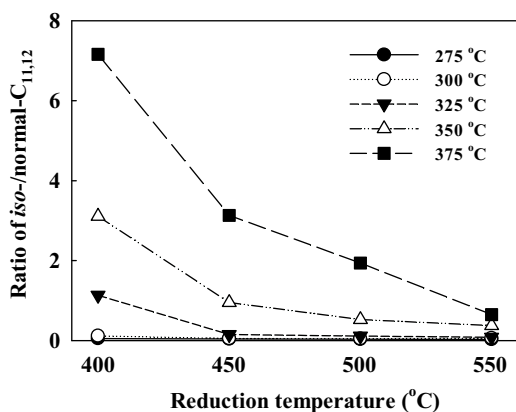


Fig. 8. Effect of the reduction temperature on the isomerization activity of the catalyst.

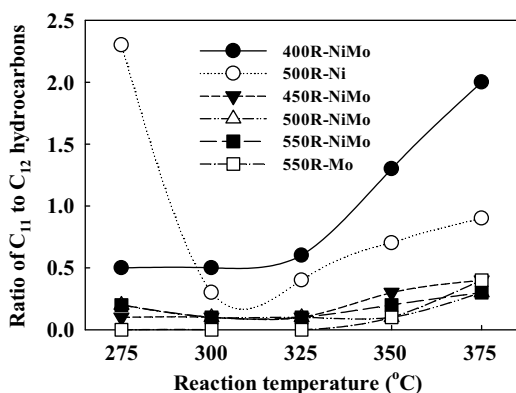


Fig. 9. Changes in the ratio of the C_{11} – C_{12} hydrocarbons as a function of reaction temperature.

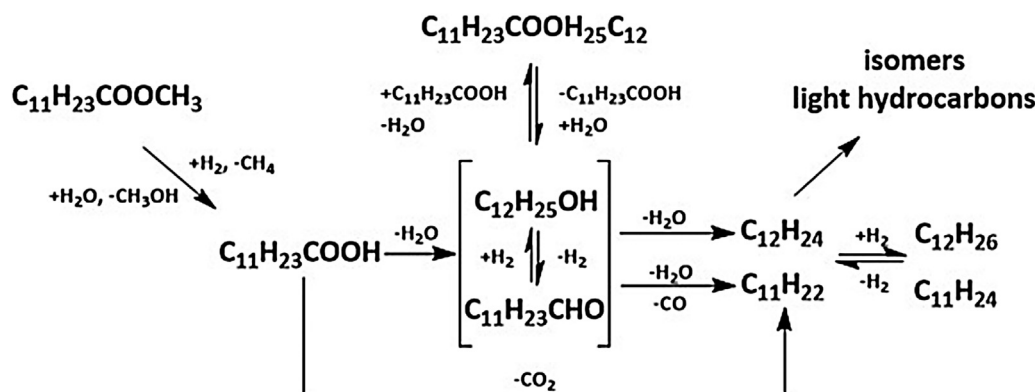
higher activity for isomerization than that of other catalysts. These results are consistent with the acidity of the catalyst (Fig. 2 and Table 3). In isomerization, the skeleton isomerization and cracking are competitive reactions, and the ratio of them is strongly dependent on the acidity of support [39]. SAPO-11 with moderate acidity was suitable as a support for long chain paraffin isomerization. In addition, the addition of another small amount of strong acid sites can promote the isomerization as well. Therefore, the new acid sites generated after reduction contribute to isomerization, and the decrease in these sites can inhibit the isomerization activity of the catalyst.

The changes in the C_{11}/C_{12} ratio that illustrate the deoxygenation pathways (HDO or DCO) are presented in Fig. 9. For the different reduction temperatures, the ratio decreased in the following order: 400R–NiMo > 450R–NiMo > 500R–NiMo > 550R–NiMo. For 500R–Ni and 400R–NiMo, the high C_{11}/C_{12} ratio suggests that DCO is the main pathway, and the oxygen atoms are nearly all removed in the form of CO or CO_2 . However, HDO was favorable over the catalyst reduced at a higher temperature (450–550 °C), with the formation of H_2O . On the other hand, the ratio over catalysts with different active metals decreased in the order of 500R–Ni > 500R–NiMo > 500R–Mo. For 550R–Mo, in particular, C_{11} hydrocarbons were not detected below a reaction temperature of 350 °C, indicating that this catalyst has a high HDO selectivity. Furthermore, the ratio increased with increasing reaction temperature, indicating that an elevated reaction temperature favors the DCO reaction. For 500R–Ni the ratio increased after the first decrease with the increasing reaction temperature. In fact, an extremely high DCO/HDO ratio (DCO selectivity > 90%) was obtained over catalysts with nickel supported on typical metal oxides, e.g., ZrO_2 , Al_2O_3 , SiO_2 or CeO_2 . However, HDO was promoted by supported zeolite (H β , HZSM-5) catalysts and strong acidity [10]. The reason for this result is not clear, but appears to be due to the presence of acid sites in the zeolite, on which the C=O bond can be adsorbed, and thus inhibit decarbonylation. Therefore, the low acid strength in SAPO-11 does not provide sufficient energy for C=O bond adsorption.

4. Discussion

4.1. HDO reaction network

Based on the product analysis, the HDO of ML is a complex process involving several reactions, i.e., hydrogenation/hydrolysis of ester, deoxygenation of intermediate oxygenates and isomerization/cracking/hydrogenation of the resulting hydrocarbons. The possible reaction network is presented in Scheme 1. First, methyl laurate was transformed into laurate acid via hydrogenation or hydrolysis, yielding methane or methanol, respectively. Secondly, the deoxygenation of laurate acid proceeded via two pathways: hydrodeoxygenation (HDO), which results in the formation of hydrocarbons with the same carbon number as the fatty acid (C_{12} hydrocarbons), and hydrodecarbonylation/decarboxylation (DCO), which results in hydrocarbons with one carbon atom less than the fatty acid (C_{11} hydrocarbons). Although only a small amount of laurate acid was observed, the amount of lauryl laurate was large (Fig. S1). The formation of lauryl laurate was resulted from the esterification of laurate acid and dodecanol. Due to the easy transformation between dodecanol and dodecanal as well as esterification, laurate acid, dodecanol and dodecanal were considered



Scheme 1. Possible reaction network for the deoxygenation and isomerization of methyl laurate.

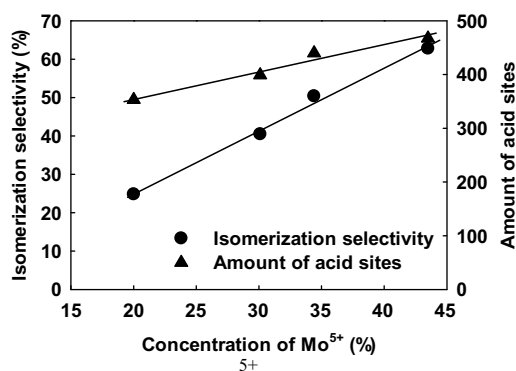


Fig. 10. Effect of Mo⁵⁺ on isomerization selectivity and the number of acid sites.

to be the key intermediates in the deoxygenation step. Finally, the deoxygenated hydrocarbons, i.e., dodecene and undecene, were further transformed into isomers and light hydrocarbons (C₅–C₁₁) via isomerization and cracking, or hydrogenated to saturated alkanes. Other kinetic studies also support this reaction network [40].

4.2. Effect of the reduction temperature on the structure and activity of the NiMo/SAPO-11 catalyst

Based on the XPS and H₂-TPR analyses, the nickel oxide was completely reduced to nickel metal in the NiMo/SAPO-11 catalyst under the studied reduction temperature (400–550 °C). However, only a portion of the nickel oxide was reduced in the Ni/SAPO-11 catalyst (Table 2). For this catalyst, the difficulty in reduction may be attributed to the high dispersion of the nickel species caused by the strong interaction between nickel and the surface –OH groups of SAPO-11. For NiMo/SAPO-11, however, two possible effects may lead to a lower dispersion of nickel species including (i) a large amount of MoO₃ loading (20 wt%) caused the subsequent loading of nickel being on the top of MoO₃. Therefore, the interaction between nickel and MoO₃ was much lower than that of SAPO-11, and caused nickel oxide to be more easily reduced; (ii) after MoO₃ loading, the surface area of SAPO-11 was dramatically reduced (from 167 to 94 m²/g). Therefore, the remaining surface area for nickel loading was much lower than that in pure SAPO-11, which resulted in the agglomeration of the metallic particles. The agglomerated nickel species are more easily reduced than the highly dispersed ones. On the other hand, it has been reported that nickel is an active metal for deoxygenation [10,11,40]. In this study, 500R-Ni exhibited a higher activity than that of 550R-Mo (Tables S2 and S3). Therefore, in contrast to the sulfided NiMo catalyst, in which NiMoS is the active site, metal nickel is considered to be more active than the reduced molybdenum species in the reduced NiMo/SAPO-11 catalyst.

On the contrary, the oxidation state of molybdenum exhibited a dramatic change in the different reduced NiMo/SAPO-11 catalysts. A lower reduction temperature (400 °C) favored the formation of Mo⁵⁺ species. When the reduction temperature increased, Mo⁵⁺

was continuously transformed to Mo⁴⁺. Massoth [41] proposed a mechanism using two Mo⁶⁺ species to explain the reduction process. After forming Mo⁵⁺, dehydroxylation leads to reduction two isolated Mo⁵⁺ to an intermediate Mo⁵⁺ pair. Interestingly, further hydrogenation of this Mo⁵⁺ pair can lead to a Mo⁶⁺ and Mo⁴⁺ species, and a site containing a vacancy is generated. These results can help explain why the amount of Mo⁶⁺ does not change much with increasing reduction temperature.

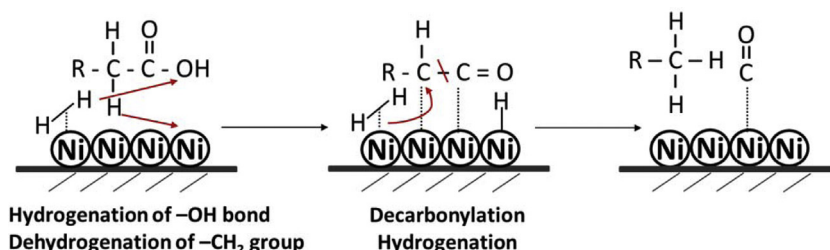
Mo⁵⁺ and Mo⁴⁺ are considered to be the isomerization and deoxygenation active sites, respectively. It has been reported that the reduced Mo/Al₂O₃ catalyst is active for a variety of reactions, such as isomerization [26,30], metathesis [42,43] and ethylene polymerization [44]. Most of these reactions require a catalyst with an acid function. The Mo⁵⁺ or Mo³⁺ species with –OH groups are considered to be Brønsted acid sites that catalyze the isomerization reaction in the hydrogenation of methyl laurate. Fig. 10 illustrates the relationships between the concentration of Mo⁵⁺ and isomerization selectivity (375 °C) as well as the amount of acid sites. Both parameters shown on the Y axis varied linearly with the Mo⁵⁺ species. In general, isomerization occurs over bifunctional catalysts containing a metallic function for hydrogenation/dehydrogenation and an acid function for skeletal isomerization via carbenium ions [45,46]. In this sense, the variation in the number of acid sites can be interpreted with the formation of Mo⁵⁺ species. Therefore, the reduction at different temperatures can alter the isomerization activity of the catalyst.

On the other hand, bulk molybdenum oxides has been explored for the hydrodeoxygenation of small oxygenates based on a reverse Mars–van Krevelen reaction (Fig. S3). The removal of the oxygen from the feedstock can occur by adsorption on the vacancy sites, i.e., the Mo⁴⁺ or Mo²⁺ species [47,48]. Both the reduced NiO/SAPO-11 and MoO₃/SAPO-11 exhibited deoxygenation activity (Table 5), indicating that both the nickel and MoO₂ species were active for the ML deoxygenation. For the NiMo/SAPO-11 catalyst, the TOF was approximately constant over the catalyst reduced at a temperature higher than 450 °C. The amount of Mo⁴⁺, however, was quite different in these catalysts. These results indicate that Mo⁴⁺ was an adsorption site rather than an active site in the reduced NiMo/SAPO-11 catalyst. Therefore, this site does not substantially affect the deoxygenation activity after reaching a certain degree.

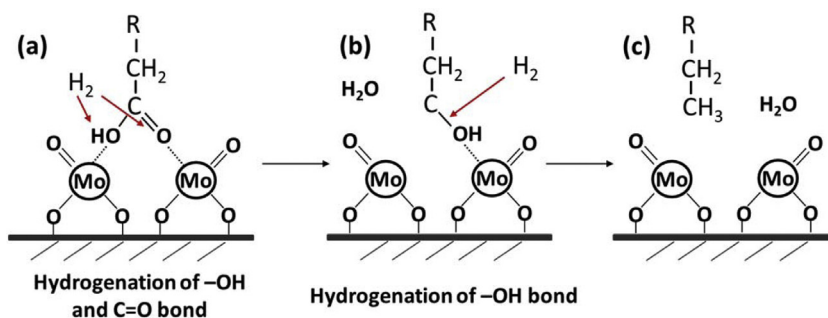
Consequently, in the NiMoO_{3-x}/SAPO-11 catalytic system, nickel provides a metallic function for deoxygenation, and the Brønsted acid sites in SAPO-11 act as an acid function. In addition, the Mo⁵⁺ in MoO_{3-x}, which has –OH functional groups, is considered to be the Brønsted acid site as well.

4.3. Deoxygenation mechanisms

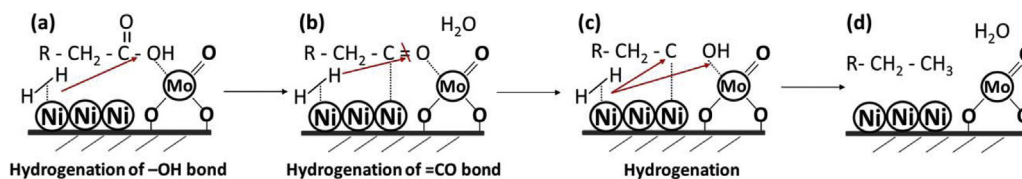
The main intermediate, lauryl laurate, can only be generated by the esterification of laurate acid and dodecanol. Therefore, laurate acid is considered to be the most abundant intermediate oxygenate and used as the initial reactant for explaining the mechanism. The activity test results indicate that the C–C bond cleavage, which



Scheme 2. Surface reaction model of C–C bond cleavage for the decarbonylation of methyl laurate over the reduced 500R-Ni catalyst.



Scheme 3. Surface reaction model of C=O hydrogenation for the hydrodeoxygenation of methyl laurate over the 550R-Mo catalyst.



Scheme 4. Surface reaction model of C=O hydrogenation for the hydrodeoxygenation of methyl laurate over the 450(500/550)R-NiMo catalyst.

results in decarbonylation, was the primarily deoxygenation pathway over the 400R-NiMo, 500R-Ni and S-NiMo catalysts, whereas the C=O bond hydrogenation, which leads to hydrodeoxygenation, is promoted by the 500R-Mo and 450(500/550)R-NiMo catalysts. The C=O hydrogenation and decarbonylation of acyl are competitive reactions that they are severely affected by the nature of the surface species. The deoxygenation mechanisms over reduced NiO/SAPO-11, MoO₃/SAPO-11 and NiMo/SAPO-11 (referring to catalysts reduced at temperature higher than 450 °C) are presented in Schemes 2–4.

- i For NiO/SAPO-11, the decarbonylation is favorable on bare nickel sites (Scheme 2). (a) First, hydrogen is dissociated, yielding two hydrogen atoms adsorbed on the nickel surface. Hydrogenation results in the transformation of a carboxylic acid to an aldehyde. (b) Meanwhile, one hydrogen atom is dehydrogenated from the carboxylic acid to the surface of the nickel, forming an adsorbed C–C bond on two adjacent nickel atoms. (c) Subsequently, the cleavage of the C–C bond occurs, and a hydrocarbon with one carbon number less than the carboxylic acid is generated. In this study, although higher DCO selectivity was observed over the 500R-Ni catalyst, the ratio of C₁₁–C₁₂ was less than 1, indicating that more C₁₂ hydrocarbons were generated compared to C₁₁. As mentioned above, the nickel supported on metal oxides, such as Al₂O₃, can achieve an extremely high DCO selectivity. Indeed, the adsorption of the C–C bond requires adjacent nickel atoms, and this kind of nickel site is not abundant on the surface of the NiO/SAPO-11 catalyst due to the high dispersion. Another reason for the lower ratio over Ni/SAPO-11 is that SAPO-11 contains a large amount of phosphorus, and the Ni₂P species can lead to the adsorption being replaced by other forms [49,50].
- ii For MoO₃/SAPO-11, the main deoxygenation pathway is hydrodeoxygenation (Scheme 3). (a) The reduction of MoO₃ can generate MoO₂, which has an oxygen vacancy. The –C=O and –OH bonds can be adsorbed on two adjacent Mo⁴⁺ species. (b) The hydrogenation of them these bonds breaks the –OH bond, resulting in the formation of the adsorbed alcohol. (c) C₁₂ hydrocarbons are generated by subsequently hydrogenating the –OH bond. The extremely high selectivity toward C₁₂ hydrocarbons (C₁₁/C₁₂ was close to zero) at a lower reaction temperature (<350 °C) suggests that the deoxygenation can only occur in this way. On the other hand, the deoxygenation activity of 550R-Mo

was much lower than the NiMo/SAPO-11 catalyst reduced at 450–550 °C (Table 5). Because the dissociated hydrogen is more difficult to generate on the molybdenum oxides than on the metal nickel.

- iii For NiMo/SAPO-11, hydrodeoxygenation is the main deoxygenation pathway, and deoxygenation activity is promoted by nickel compared to MoO₃/SAPO-11. The ratio of C₁₁–C₁₂ was similar over 450(500/550)R-NiMo, while 400R-NiMo showed higher decarbonylation selectivity than other three reduced NiMo/SAPO-11 catalysts. This result indicates that the deoxygenation mechanism is different for 400R-NiMo and 450(500/550)R-NiMo. In 400R-NiMo, the amount of Mo⁴⁺ (27.6%) was low, and thus the number of adsorption sites for the C=O group was in low supply, which results in little hydrodeoxygenation over this catalyst. Therefore, metal nickel catalyzed decarbonylation became the dominant pathway. In contrast, the NiMo/SAPO-11 catalyst reduced above 450 °C exhibited a similarly high C₁₁/C₁₂ ratio compared to reduced MoO₃/SAPO-11, indicating that the deoxygenation mechanism was similar over these catalysts (Scheme 4). (a) First, the –OH group of the carboxylic acid is hydrogenated on the Ni or Mo⁴⁺ sites, resulting in the formation of an intermediate aldehyde. (b) Then the C=O bond in the aldehyde is adsorbed on Mo⁴⁺. The partially reduced molybdenum species, i.e., Mo⁴⁺, can be considered as Lewis acid site, and thus the carbonyl group can be easily adsorbed on an electron acceptor rather than on the nickel site. (c) Hydrogenation of the C=O bond by the dissociated hydrogen generated from the adjacent nickel sites occurs, resulting in the formation of C₁₂ hydrocarbons and adsorbed –OH group on Mo⁴⁺. (d) Finally, hydrogenation of the adsorbed –OH groups can transform the molybdenum species into the initial form. In short, the co-presence of metallic Ni species and partially reduced MoO₂ may be responsible for the high HDO selectivity and deoxygenation activity.

5. Conclusions

This study demonstrated an effective non-sulfide and non-noble metal catalyst, NiMo_{3-x}/SAPO-11, for the one step deoxygenation and isomerization of methyl laurate to high isomer containing hydrocarbons. The effect of the reduction temperature on the structure of the catalyst and their performance was investigated. The

characterization results from H₂-TPR and XPS indicate that nickel oxides were completely reduced to nickel metal, whereas the molybdenum species exhibited a different distribution of valences after reduction at different temperatures. The catalyst reduced at 400 °C showed the highest isomerization selectivity due to its higher amount of acid sites. However, an elevated reduction temperature decreased the concentration of the Mo⁵⁺ species and the amount of acid sites as well, resulting in a lower selectivity toward isomerization. On the other hand, the catalyst reduced at 400 °C favored the decarbonylation pathway due to nickel-catalyzed C–C bond cleavage, whereas C=O bond hydrogenation was favored over catalysts reduced at higher temperatures. Consequently, the NiMo_{3-x}/SAPO-11 catalyst reduced at 450 °C possessed a good balance between its deoxygenation activity and isomerization selectivity, and exhibited a synergetic effect on hydrodeoxygenation due to the of nickel metal and Mo⁴⁺ species.

Appendix A. Supplementary data

Supplementary data associated with this article can be found, in the online version, at <http://dx.doi.org/10.1016/j.apcatb.2015.03.011>.

References

- [1] C. Zhao, T. Brück, J.A. Lercher, *Green Chem.* 15 (2013) 1720.
- [2] D. Kubicka1, I. Kubickova1, J. Cejka, *Catal. Rev. Sci. Eng.* 55 (2013) 1.
- [3] G.W. Huber, P. O'Connor, A. Corma, *Appl. Catal. A* 329 (2007) 120.
- [4] S. Gong, A. Shinozaki, M. Shi, E.W. Qian, *Energy Fuels* 26 (2012) 2394.
- [5] D. Kubicka, J. Horacek, *Appl. Catal. A* 394 (2011) 9.
- [6] T.-R. Viljava, E.R.M. Saari, A.O.I. Krause, *Appl. Catal. A* 209 (2001) 33.
- [7] O.V. Kikhtyanin, A.E. Rubanov, A.B. Ayupov, G.V. Echevsky, *Fuel* 89 (2010) 3085.
- [8] M. Ahmadi, E.E. Macias, J.B. Jasinski, P. Ratnasamy, M.A. Carreon, *J. Mol. Catal. A* 386 (2014) 14.
- [9] C. Wang, Z. Tian, L. Wang, R. Xu, Q. Liu, W. Qu, H. Ma, B. Wang, *ChemSusChem* 5 (2012) 1974.
- [10] B. Peng, X. Yuan, C. Zhao, J.A. Lercher, *J. Am. Chem. Soc.* 134 (2012) 9400.
- [11] B. Peng, Y. Yao, C. Zhao, J.A. Lercher, *Angew. Chem. Int. Ed.* 51 (2012) 2072.
- [12] B. Peng, C. Zhao, S. Kasakov, S. Foraita, J.A. Lercher, *Chem. Eur. J.* 19 (2013) 4732.
- [13] N. Chen, S. Gong, E.W. Qian, *Jpn. Pet. Inst.* 56 (2013) 249.
- [14] T. Kabe, W. Qian, Y. Hirai, L. Lai, A. Ishihara, *J. Catal.* 190 (2000) 191.
- [15] V.M. Akhmedov, S.H. Al-Khowaiter, *Catal. Rev.* 49 (2007) 33.
- [16] S. Brunauer, P.H. Emmett, E. Teller, *J. Am. Chem. Soc.* 60 (1938) 309.
- [17] E.P. Barrett, L.G. Joyner, P.P. Halenda, *J. Am. Chem. Soc.* 73 (1951) 373.
- [18] N. Chen, S. Gong, H. Shirai, T. Watanabe, E.W. Qian, *Appl. Catal. A* 466 (2013) 105.
- [19] E.W. Qian, N. Chen, S. Gong, *J. Mol. Catal. A* 387 (2014) 76.
- [20] A.C. Faro, P. Grangeb, S.K. Maity, *Appl. Catal. A* 471 (2014) 28.
- [21] L. Chiuping, C. Yu-Wen, *Thermochim. Acta* 256 (1995) 457.
- [22] H. Sakagami, T. Ohno, H. Itoh, Z. Li, N. Takahashi, T. Matsuda, *Appl. Catal. A* 470 (2014) 8.
- [23] W. Suarez, J.A. Dumesic, C.G. Hill, *J. Catal.* 94 (1985) 408.
- [24] M. Yamada, J. Yasumaru, M. Houalla, D.M. Hercules, *J. Phy. Chem.* 95 (1991) 7037.
- [25] I. Oliveros, M.J. Perez Zurita, C. Scott, M.R. Goldwasser, J. Goldwasser, S. Rondon, M. Houalla, D.M. Hercules, *J. Catal.* 171 (1997) 485.
- [26] F. Barath, M. Turki, V. Keller, G. Maire, *J. Catal.* 185 (1999) 1.
- [27] Y. Holl, R. Touroude, G. Maire, A. Muller, P.A. Engelhard, J. Grosmangin, *J. Catal.* 104 (1987) 202.
- [28] W. Grunert, A.Y. Stakheev, W. Morke, R. Feldhaus, K. Anders, E.S. Shpiro, K.M. Minachev, *J. Catal.* 135 (1992) 269.
- [29] V. Keller, F. Barath, G. Maire, *J. Catal.* 189 (2000) 269.
- [30] F.E. Massoth, *Adv. Catal.* 27 (1978) 265.
- [31] L. Portela, P. Grange, B. Delmon, *Catal. Rev. Sci. Eng.* 37 (4) (1995) 699.
- [32] X. Wang, U.S. Ozkan, *J. Catal.* 227 (2004) 492.
- [33] A.Y. Bunch, X. Wang, U.S. Ozkan, *Appl. Catal. A* 346 (2008) 96.
- [34] M. Mihaylov, K. Hadjiivanov, *Langmuir* 18 (2002) 4376.
- [35] L. Boda, G. Onyestyak, H. Solt, F. Lonyi, J. Valyon, A. Thernes, *Appl. Catal. A* 374 (2010) 158.
- [36] O.I. Senol, E.-M. Ryymin, T.-R. Viljava, A.O.I. Krause, *J. Mol. Catal. A* 268 (2007) 1.
- [37] B. Donnis, R.G. Egeberg, P. Blom, K.G. Knudsen, *Top. Catal.* 52 (2009) 229.
- [38] H. Deldari, *Appl. Catal. A* 293 (2005) 1.
- [39] P. Kumar, S.R. Yenumala, S.K. Maity, D. Shee, *Appl. Catal. A* 471 (2014) 28.
- [40] E.E. Massoth, *J. Catal.* 30 (1973) 204.
- [41] P.A. Engelhard, J. Goldwasser, W.K. Hall, *J. Catal.* 76 (1982) 48.
- [42] D. Zhang, X. Li, S. Liu, X. Zhu, F. Chen, L. Xu, *Appl. Catal. A* 472 (2014) 92.
- [43] G.K. Borekov, V.A. Dzisko, V.M. Emel-Yanova, Y.I. Pecherskoy, *Dolk. Akad. Nank.* 150 (1963) 829.
- [44] J.A. Martens, M. Tielen, P.A. Jacobs, *Stud. Surf. Sci. Catal.* 46 (1989).
- [45] X. Wang, C. Li, Y. Wang, T. Cai, *Catal. Today* 93–95 (2004) 135.
- [46] D.R. Moberg, T.J. Thibodeau, F.G. Amar, B.G. Frederick, *J. Phys. Chem. C* 114 (2010) 13782.
- [47] T. Prasomesri, T. Nimmanwudipong, Y. Ronman-Leshkov, *Energy Environ. Sci.* 6 (2013) 1732.
- [48] H. Song, J. Wang, Z. Wang, H. Song, F. Li, Z. Jin, *J. Catal.* 311 (2014) 257.
- [49] J. Moon, E. Kim, Y. Lee, *J. Catal.* 311 (2014) 144.